Effect of Slot-Pole Numbers on the Performance of a BLDC Motor for Agro-EV Application

Muhammad Izanie Kahar[1], **Raja Nor Firdaus Kashfi Raja Othman**[1†], **Aziah Khamis**[1], **Nurfaezah Abdullah**[1], **Fairul Azhar Abdul Shukor**[1], and **Lim Seng Tat**[2], Non-members

ABSTRACT

This paper analyzes the performance of a brushless direct current (BLDC) motor for agro electric vehicle (agro-EV) applications. Agro-EV technology is being developed in response to increasing environmental pollution. Various types of electric motors are in agro-EV, one of which is the BLDC. With its good capabilities, it has been chosen for further exploration in this research. On the other hand, some issues limit the usage of the conventional BLDC motor in heavy applications, such as low torque performance caused by weak magnetic energy. Therefore, this research aims to analyze the effect of magnetic energy based on slot-pole combinations to evaluate the BLDC motor's performance. Three BLDC models with different slot-pole numbers are designed and simulated using a fixed structure size, permanent magnet volume, and magnetomotive force (MMF). Finite element method (FEM) software known as Altair Flux 2D is used to compute the cogging torque, back-electromotive force (BEMF), magnetic flux density, and the torque produced. As a result, an 18/20 slot-pole was chosen for its high torque (105 Nm) and BEMF (35.9 V). In conclusion, this research simulation presents guidelines and an overview regarding the effect of slot-pole numbers on the performance of the BLDC motor for agro-EV applications.

Keywords: Brushless Direct Current Motor, BLDC, Altair Flux 2D, Torque, Agro-EV

1. INTRODUCTION

In this new era, small electric vehicle technology is being widely developed for the benefits of its low-pollution system to the environment. Today's generations are really concerned about the environment, particularly noise and carbon emissions [1–3]. In order to have clean air, everyone should opt for electrical-based vehicles. The primary advantage of agro-EVs relates to the location of the electric motor which is powered up electronically [2, 4]. Various electric motors are used for agro-EVs, one of which is the permanent magnet brushless DC motor (PM BLDC) [5–7]. The BLDC motor is known for its good performance and thus can be used in a wide range of applications. The agro-EV's performance depends on the efficiency of its electric motor [2, 3, 8–10]. Furthermore, the BLDC motor produces less noise during operation which reduces sound pollution, and it is also suitable for long-term usage while maintaining efficiency since there is no winding at the rotor or copper losses [11–13].

As more research is conducted on the BLDC motor, more defects seem to appear. The structure of the BLDC has a major influence on its performance. The lack of a properly built structure can lead to deterioration of the BLDC motor's performance [14, 15]. Besides, conventional BLDC motors are less capable in heavy applications due to their poor performance [13, 16]. It is crucial for agro-EVs to have high torque performance since they are used for transportation. Furthermore, a good performing BLDC motor should have low cogging torque, high back-electromotive force (BEMF), and high torque density [17–19]. However, due to the lack of magnetic energy, the torque produced by the BLDC motor is still insufficient. This is possibly due to the unsuitable combination of slot and pole numbers of the BLDC motor [20, 21].

Therefore, studies have been conducted on the use of different numbers of slots and poles on the BLDC motor. For instance, a recent study by Cabuk *et al.* [22] discussed the impact of varying slot-pole combinations on the output power, along with iron and core losses. In that study, the optimum design of the BLDC motor for in-wheel light electric vehicle (LEV) propulsion was presented. The optimization work was mainly based on different slot-pole numbers, which gave substantial performance improvement in certain applications. The BLDC motor experienced high cogging torque, reducing its performance. Another study by Garniwa *et al.* [23] analyzed the thermal issue effect of slot-pole variation. The methods used to analyze the temperature inside the motor consisted of laboratory experiments and EV field tests. The motor had low torque performance due to magnetic energy loss. Meanwhile, Krotsch *et al.* [24] explored different slot and pole number combinations with diverse spatial and specific frequency harmonic ordinal numbers. The research discussed the radial

Manuscript received on February 9, 2021; revised on April 15, 2021; accepted on September 21, 2021. This paper was recommended by Associate Editor Yuttana Kumsuwan.

[1]The authors are with the Electrical Machine Design Research Laboratory, Centre of Robotics and Automation (CeRIA), Faculty of Electrical Engineering, Universiti Teknikal Malaysia Melaka (UTeM), 76100 Durian Tunggal, Melaka, Malaysia.

[2]The author is with the Altair Engineering Sdn. Bhd., 50470 Kuala Lumpur, Malaysia.

[†]Corresponding author: norfirdaus@utem.edu.my

Digital Object Identifier: 10.37936/ecti-eec.2022201.246104

Table 1: *PM BLDC design specifications.*

Design Consideration	Value
Input voltage, V	48 V
Input current, I	10 A
No. of phases	3
Input power, P	1440 W
Rotational speed, ω	200 rpm

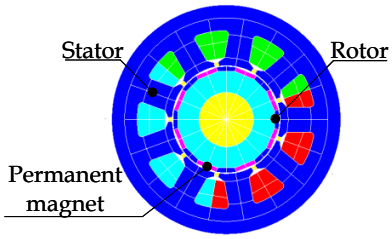

Fig. 1: *Basic structure of the PM BLDC motor.*

magnetic force harmonics influenced by the stator tooth structure, pole-arc coefficient, and permeability of PM, while the validity and accuracy of the analysis results were verified by experimental tests.

This research discusses in detail the effect of optimizing magnetic energy in agro-EV application on the BLDC motor's performance. Therefore, the proposed PM BLDC focuses on different slot and pole models, analyzing the cogging torque, BEMF, torque produced, and magnetic flux density. Altair Flux 2D is used to compute the simulation of the BLDC motor and analysis in terms of its performance and improvement for agro-EV application.

2. BASIC BLDC STRUCTURE

In this research, the agro-EV requires high torque and BEMF for efficient usage. The design specifications are listed in Table 1. The analysis focuses on three models involving configurations with different numbers of slots and poles, i.e., 18/20, 12/10, and 9/8 slot-poles. These slots and poles were chosen based on fractional slots and three-phase winding topology. The pole number was chosen to be close to the number of slots to ensure uniform and continuous distribution of magnetic energy and force in the motor. The basic structure of the BLDC motor is shown in Fig. 1.

As shown in Fig. 2, the input voltage and current use the DC source from the battery. This will subsequently be converted into AC for the BLDC motor to operate in the three-phase system. One of the features of the target motor in this research is it is a BLDC with a sinusoidal BEMF.

Furthermore, the BLDC motor in this research is specifically for light application in agriculture, i.e., an electric wheelbarrow. As shown in Fig. 3, the BLDC motor needs a high torque to move the load from one place to another. Since it is intended for a light application, the input current source does not need to be high since the BLDC motor must consider the heat factor.

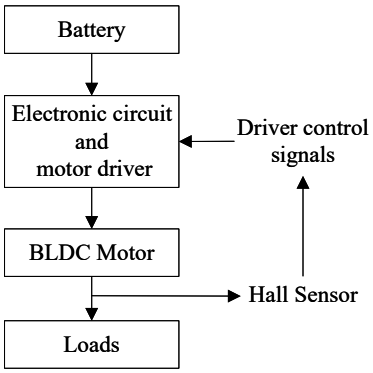

Fig. 2: *Block diagram of the agro-EV system.*

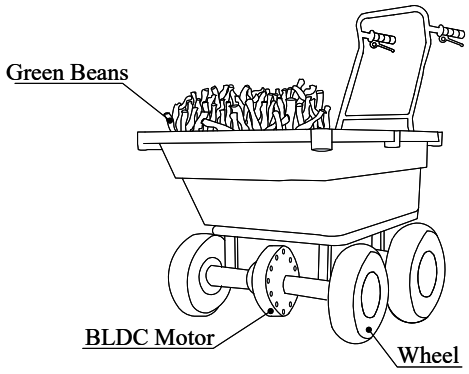

Fig. 3: *Desired application for this motor.*

2.1 Research Methodology

The research methodology was separated into two parts, namely, designing the PM BLDC motor and analyzing the transient magnetic application under several conditions. The overall methodology used in this research is shown in Fig. 4. The sizing parameters of the model were determined based on the required design specification. To develop the models as required, two methods were used, i.e., calculation and FEM. The parameters for the PM BLDC motor size were determined through calculation. The modeling process then continued using the FEM. Each model was computed under different conditions using the FEM to study the wider effects and explain the reasons behind them. The analysis on cogging torque, BEMF, electromagnetic torque, and magnetic flux density was conducted for different models of the PM BLDC motor. The analysis results of each model were evaluated based on the required criteria and the best model subsequently selected. The model configurations considered in this research were 9/8, 12/10, and 18/20 slot-poles, with the process starting with the 9/8 slot-pole model configuration, as shown in Fig. 4.

2.2 Motor Sizing

The stator and rotor size was determined using the conventional design method [25]. The model was designed with fixed parameters, i.e., stator and rotor outer radius, rotor shaft, air gap, and stack length. As

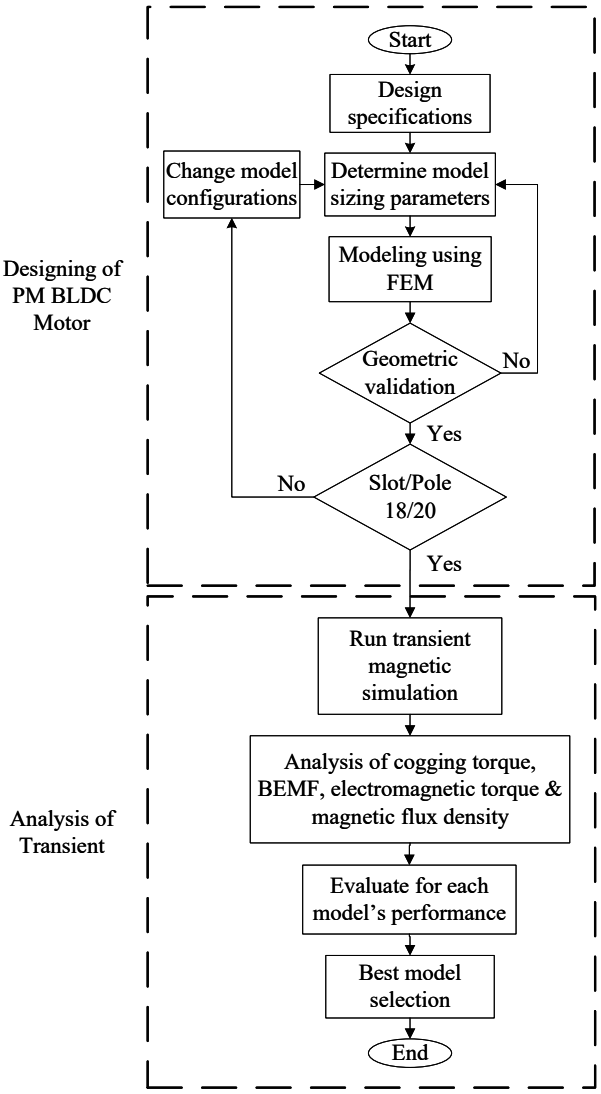

Fig. 4: *Overall methodology.*

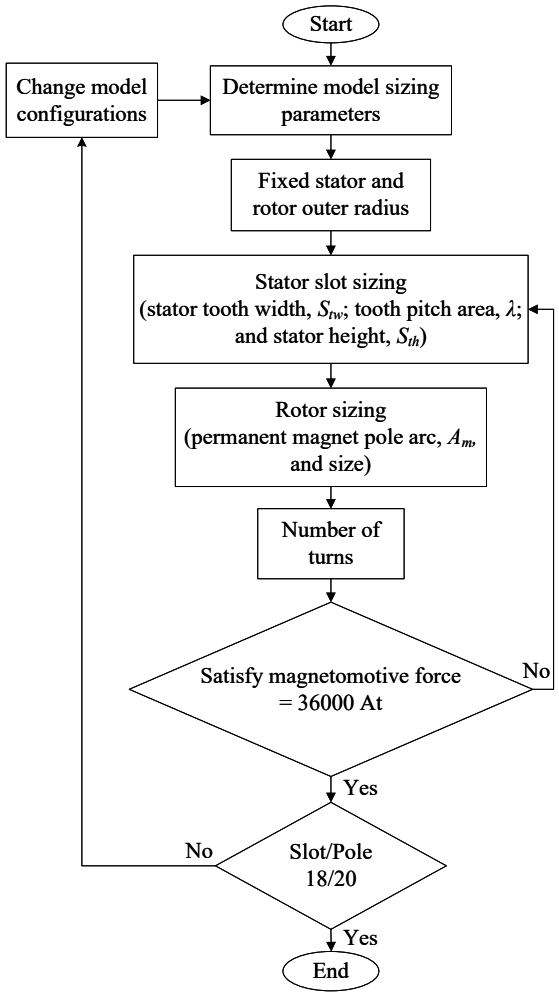

Fig. 5: *Flowchart of motor sizing used in this paper.*

can be observed in Fig. 5, the sizing starts with a fixed stator and rotor of 160 mm and 74.5 mm, respectively. The model configurations considered were 9/8, 12/10, and 18/20 slot-poles, starting with a 9/8 slot-pole, as presented in Fig. 5.

Next, the calculation proceeded with the basic dimension, namely the stator tooth width, S_{tw}. The stator tooth width was calculated as,

$$S_{tw} = \tau \times \lambda \qquad \text{(mm)} \qquad (1)$$

where τ is the ratio of stator tooth width over tooth pitch with its value fixed to 0.5 and λ is the tooth pitch value measured from the middle of the stator slot as shown in Fig. 6(a). The λ value depends on the number of stator slots with a fixed stator circumference of 1005 mm. The stator height was then determined based on the flow path of its flux. As can be observed in Fig. 6(a), the stator flux $_1$ and $_2$ will flow through the stator tooth width and be divided into two parts to obtain the stator height, S_{th}. The stator height was defined using

$$S_{th} = \frac{1}{2} \times S_{tw} \qquad \text{(mm)} \qquad (2)$$

The stator height (A_2) is considered as half the stator tooth width (A_1), where the width of A_1 is equivalent to $2A_2$ as shown in Fig. 6(b).

To ensure the balance of magnetic flux distribution in the stator, the total permanent magnet surface area used must be fixed for all models. It is important to identify the permanent magnet pole arc due to the different numbers of poles used in the fixed rotor size. Therefore, the permanent magnet pole arc depends on the calculated length of the permanent magnet. The width and surface area of the permanent magnet were fixed at 6 mm and 1440 mm^2, respectively. The permanent magnet pole arc was determined using

$$A_m = \frac{\text{Permanent magnet surface area}}{\text{Number of poles}} \qquad (\text{mm}^2) \qquad (3)$$

$$L_m = \frac{A_m}{\text{Magnet width}} \qquad \text{(mm)} \qquad (4)$$

$$\text{Magnet pole arc} = \sqrt{\frac{L_m}{360}} \qquad \text{(deg)} \qquad (5)$$

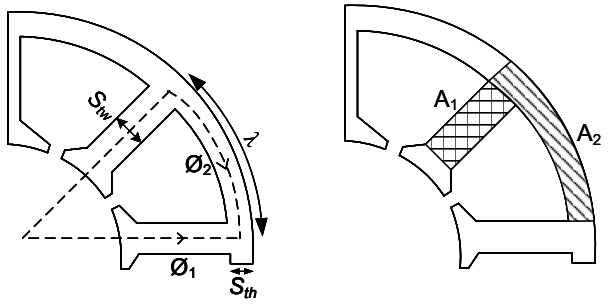

(a) (b)

Fig. 6: *Stator tooth width (S_{tw}) and stator tooth height (S_{th}); (a) cross-section and (b) size.*

where A_m is the permanent magnet surface area per pole and L_m is the permanent magnet length. The number of turns of a coil (N) must be suitable for the stator, as defined in Eq. (6)

$$N = \frac{W_{coil} \times H_{coil}}{D_{coil}} \times 60\% \qquad \text{(turns)} \qquad (6)$$

where W_{coil} is the coil width, H_{coil} is the coil height, and D_{coil} is the coil diameter. The coil fill factor was fixed at 60%.

All three models were considered to have the same value of magnetomotive force (MMF), i.e., 36000 At (ampere-turns); the highest limit for the subsequent analysis. The MMF value was calculated based on the 18/20 slot-pole using

$$\text{MMF} = N \times I \times \text{No. of slots} \qquad \text{(At)} \qquad (7)$$

In order to achieve the desired value of MMF for other models, the input current must be determined. The input current (I) was computed using Eq. (7).

The designed parameters for all three models of the PM BLDC motor are tabulated in Table 2. The stator and rotor radius, stack length, and air gap value were kept the same. The mechanical air gap between the inner stator and outer rotor prevented the stator and rotor from colliding with each other. The volume of the permanent magnet and MMF was fixed for all models to ensure equal distribution of the magnetic flux in the stator.

2.3 FEM Modeling Simulation

In this paper, the FEM was used to obtain a visual overview (2D sketching) of the required structure based on the design parameters. The accuracy and efficiency of the system should be demonstrated by the expected visual output. The FEM modeling started with geometry sketching based on the calculated design parameters. For these models, the square and spoke type stator and rotor are shown in Table 2. The final models for each different motor are presented in Fig. 7. The following operation was meshed by rendering the physical geometry. The mesh was used to identify an improperly built motor

Table 2: *Design parameter of the PM BLDC motor for three different slots and poles.*

Parameter	Motor 1	Motor 2	Motor 3
Slots and poles	18/20	12/10	9/8
Rotor type	Rotor spoke		
Shaft radius (mm)	38		
Rotor outer radius (mm)	74.5		
Magnet width (mm)	6		
Magnet pole arc (deg)	95	90	88
Magnet type	Not embedded		
Pole number	20	10	8
Stator type	Square		
Stator tooth width (mm)	19	24	38
Stator slot	18	12	9
Stator outer radius (mm)	160		
Winding turns	200	300	307
Maximum input current (A)	10	10	13
Magnetomotive Force (At)	36000		
Air gap (mm)	1		
Stack length (mm)	105		

structure. This was achieved by dividing the object into smaller triangular pieces using a partial differential equation to ease the solving process, as shown in Fig. 8. It also provided a detailed calculation for the FEM software to subsequently compute the analysis with high accuracy. The more detailed the mesh, the higher the accuracy of the results. After completing the mesh generation process, the physical description of the motor was defined. In this paper, the permanent magnet material consisted of neodymium boron iron (NdFeB), whereas the rotor and stator used steel. Lastly, the model underwent geometry checking. If an error occurs and the geometry is not satisfied, the design parameters will be rechecked or changed to a new value.

3. TRANSIENT MAGNETIC SIMULATION

The PM BLDC was analyzed using the FEM. To analyze the models based on the magnetic effect, the transient magnetic simulation application was used. Various values of speed and input current were used in this research. External circuits were also used to represent the motor physics. Upon completion of the computation, the results of cogging torque, BEMF, electromagnetic torque, and magnetic flux density were analyzed. The performance of each model was evaluated and a suitable model selected for agro-EV application.

The cogging torque was simulated with various positions for the zero-input current. The speeds used for the analysis were 200, 400, 600, 800, and 1000 rpm. To obtain the period of cogging torque, the angle of the rotor must be varied over a slot pitch. The period of cogging torque is expressed by

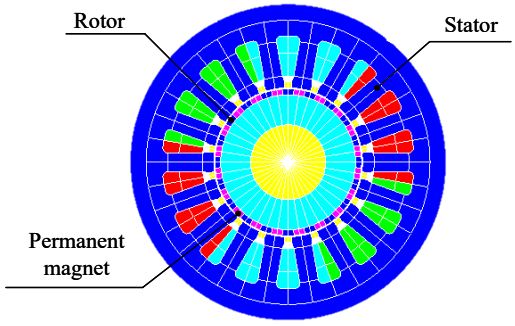

(a) 18/20 slots and poles (Motor 1)

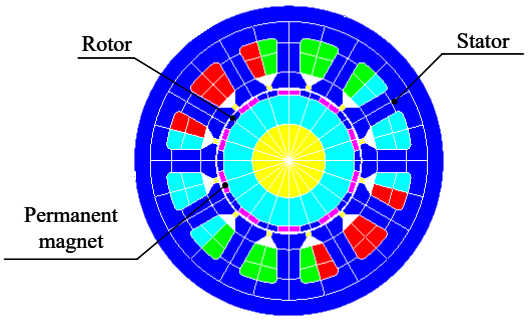

(b) 12/10 slots and poles (Motor 2

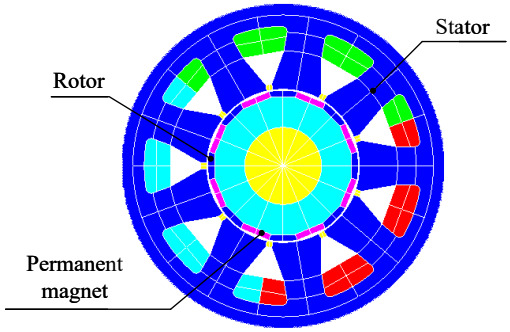

(c) 9/8 slots and poles (Motor 3

Fig. 7: *Simulation model with three different slots and poles.*

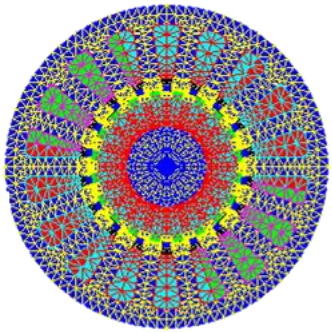

(a) 18/20 slots and poles (Motor 1)

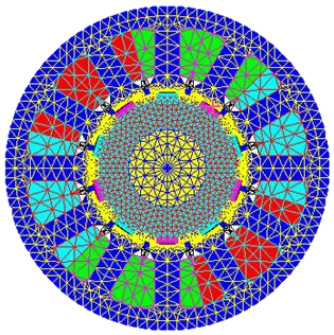

(b) 12/10 slots and poles (Motor 2

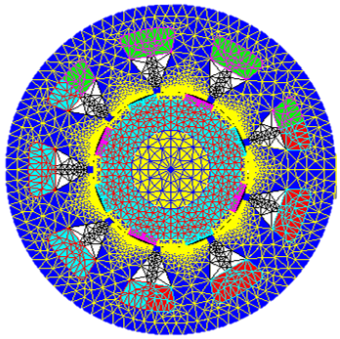

(c) 9/8 slots and poles (Motor 3

Fig. 8: *Meshed physical geometry.*

$$\text{Period of cogging torque} = \frac{360}{\text{LCM}\,(n_r,\, n_s)} \quad \text{(mech. deg)} \tag{8}$$

where LCM is the least common multiplier, n_r is the number of rotor poles, and n_s is the number of stator slots.

Next, to obtain the BEMF vs. speed, an external circuit with components was used to represent the motor parts. To compute the BEMF, the input current was set to 0 A. During this state, it corresponded to the motor being in the generator mode with no load connection. The stranded coil conductors and inductances represented the stator coils, while the resistance acted as the resistance of the generator itself. To compute the BEMF, a large resistance value was set, i.e., 10 kΩ. Fig. 9 illustrates the external circuit used. The three components in each series line corresponded to the three-phase configuration of the motor. The speeds used for the computation were 200, 400, 600, 800, and 1000 rpm. The BEMF period depends on the pole number of the rotor. It can be expressed as

$$\text{Period of BEMF}_{\text{mech}} = \frac{360}{\text{No. of poles}} \times 2 \quad \text{(mech. deg)} \tag{9}$$

where the BEMF period represents the mechanical degree, equivalent to a complete electrical degree cycle. The control angle between the phase currents corresponding to the phase BEMF was also determined. The control angle represents half the period of the BEMF obtained and can be expressed as the equivalent electrical degree as depicted in Eq. (10).

$$\text{Period of BEMF}_{\text{elec}} = \text{Period of BEMF}_{\text{mech}} \times \text{Poles pairs} \tag{10}$$

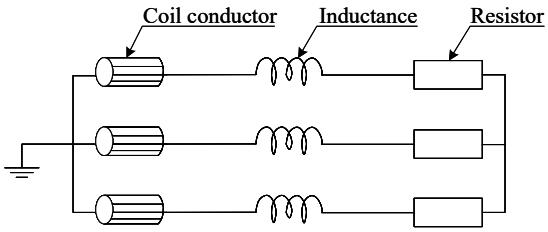

Fig. 9: *External circuit representing parts of the motor for BEMF computation.*

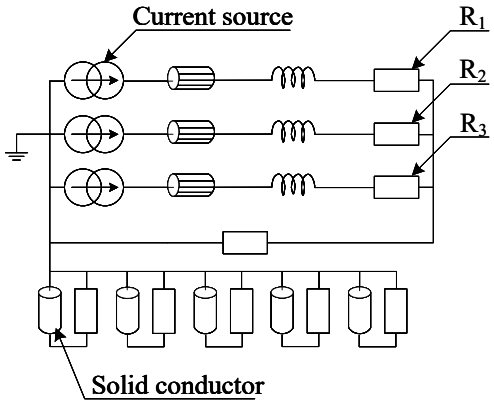

Fig. 10: *External circuit representing parts of the motor for constant speed computation.*

The current source was used for the electromagnetic torque, simulated using constant speed computation. The simulation used a constant speed of 200 rpm with various input currents. The current control angle obtained in the BEMF analysis was applied in this simulation to achieve the maximum torque it can produce. The current control angle was used to ensure the phase input current was aligned with the BEMF to obtain a high torque value. By using the previous external circuit (Fig. 9), additional solid conductors and resistors could be employed, as shown in Fig. 10. The eddy current in the permanent magnet was present in this model. To eliminate the eddy current, the permanent magnet, representing the solid conductors connected in series with a large resistance, was fixed at 10 kΩ. The number of solid conductors and resistances added was based on the number of poles in the model. The R_1, R_2, and R_3 values were changed to 0.001 Ω since the motor was now simulated with no load. The final torque comparison was made during each different slot-pole model with equal MMF, namely 36000 At. Therefore, the current inputs used for this simulation were 2 A, 4 A, 6 A, 8 A, 10 A, and 13 A.

The magnetic flux density was analyzed by executing the iso values with plots of color shading. After the computation had been completed, the magnetic flux density was observed in all parts of the model. As can be observed from Fig. 11, the analysis was performed by matching the plot of color shading with the selected part of the model's face region. In this research, the region selected for analysis was at the middle of the

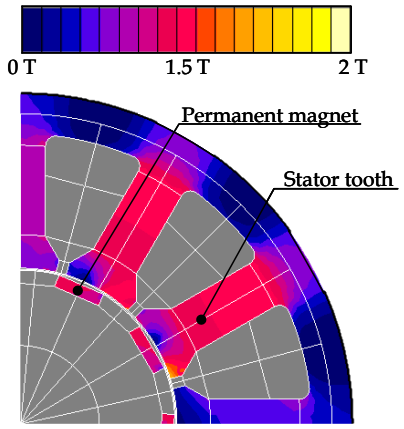

Fig. 11: *Color shading of the magnetic flux density at the stator tooth.*

stator tooth used for coil winding and had the highest value. The lighter colors of shading corresponded to the high magnetic flux density value and vice versa. The stator's magnetic flux density for each different model was analyzed at input currents of 2 A, 4 A, 6 A, 8 A, 10 A, and 13 A.

The performance was observed by analyzing the torque-speed characteristics of the BLDC motor. One characteristic of the BLDC motor is that the torque is inversely proportional to the speed. These two crucial factors should be considered when developing a BLDC to ensure it is suitable for agro-EV application. A good agro-EV should have a high torque value at low speed. The values of the torque-speed characteristic depend on Eqs. (11)–(13),

$$T_{stall} = \frac{K_T V}{R} \quad \text{(Nm)} \tag{11}$$

$$\omega_{no-load} = \frac{V}{K_e} \quad \text{(rpm)} \tag{12}$$

$$R_{coil} = \rho \frac{l}{A} \quad (\Omega) \tag{13}$$

where T_{stall} is the stall torque (Nm), $\omega_{no-load}$ is the speed during no-load (rpm), K_T is the torque constant, K_e is the constant of the BEMF, V is the input voltage (V), R is the coil resistance (Ω), ρ is the coil resistivity (Ω/km), and l and A are the length (m) and area (mm^2) of the coil, respectively.

Finally, all three slots and poles of the PM BLDC were analyzed for performance. The cogging torque, BEMF, electromagnetic torque, and magnetic flux density were evaluated. The model with the highest BEMF and electromagnetic torque was selected as the best model for agro-EV application.

4. PERFORMANCE OF THE BLDC MOTOR

4.1 Cogging Torque

Fig. 12(a) shows the waveform of the cogging torque, T_C. The period of the cogging torque depends on the

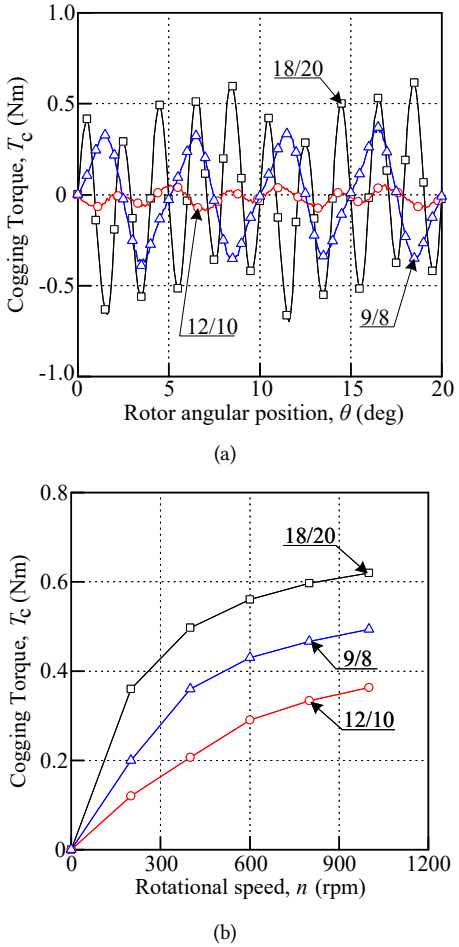

Fig. 12: *Cogging torque; (a) waveform and (b) average value.*

slot and pole number combinations. The 18/20 slot-pole varied over two mechanical degrees per slot pitch to make one complete electrical degree cycle, whereas the 12/10 and 9/8 slot-poles required six and five mechanical degrees per slot pitch, respectively.

Among the remainder, the 18/20 slot-pole obtained the highest cycle since it had the highest slot and pole number. This uneven peak was possibly due to the permanent magnet sizing and structure of the rotor and stator. It could also be due to the slot opening width or air gap length, potentially causing a non-uniform air gap between the rotor and stator.

Fig. 12(b) shows the average cogging torque value from the model simulation using different rotational speeds with zero-input current. As can be observed, the cogging torque increases proportionally with the rotational speed increment. The results revealed that at the lowest speed of 200 rpm, the 18/20 and 12/10 slot-poles had the highest and lowest cogging torque of 0.36 Nm and 0.12 Nm, respectively, whereas the 9/8 slot/pole obtained a cogging torque of 0.2 Nm. This trend continued to rise as the rotational speed increased.

On the other hand, at a speed of 1000 rpm, the 18/20 slot-pole obtained 0.62 Nm, while the 12/10 and 9/8 slot-poles obtained 0.36 Nm and 0.49 Nm, respectively. This demonstrated that the 18/20 slot-pole had the highest cogging torque, and the 12/10 slot-pole had the lowest from the start. The cogging torque increment was not affected by the increase in speed due to the magnetic energy being influenced by the slot-pole number. A higher number of slots and poles contribute to higher magnetic energy which may result in higher cogging torque.

In addition, although the 9/8 slot-pole was expected to have the lowest cogging torque, it reached 12/10 slot-pole configurations. Meanwhile, the 12/10 slot-pole is larger than the 9/8 slot-pole configuration. This is because the structure of stator and rotor of the 12/10 slot-pole itself seems to be better designed than the 9/8 slot-pole configurations (Figs. 7(b) and 7(c)). The unsuitable shape of the stator tooth in the 9/8 slot-pole results in unusable space for the windings and uneven structure of the rotor, disrupting the air gap and causing the rotor and stator to collide with each other.

It can be concluded that the 18/20 slot-pole had the highest cogging torque due to its slot and pole numbers, whereas the 9/8 slot-pole was the second-highest due to the structure of its rotor and stator.

4.2 Back-Electromotive Force (BEMF)

Fig. 13(a) shows the sinusoidal waveform of the BEMF at a constant speed of 200 rpm for each slot-pole model. Each model's position varied, depending on the number of slot-pole configurations. Larger configurations required smaller angles of mechanical degree to make one complete electrical cycle. The 18/20 slot-pole needed 36 mechanical degrees, while the 12/10 and 9/8 slot-poles required 72 and 90, respectively. The computed BEMF was used to determine the current control angle between the input phase currents and corresponding BEMF phase. For the 18/20, 12/10, and 9/8 slot-poles, the control angle between the phase currents was 18, 36, and 45 degrees, respectively.

All of these values were obtained using Eq. (9). An equivalent electrical cycle with respect to the mechanical degree control angle of the 18/20, 12/10, and 9/8 slot-poles was 180 degrees, which was obtained using Eq. (10).

Fig. 13(b) illustrates the RMS value of the BEMF for each model against the increasing rotational speed. The BEMF of all three models increased linearly as the rotational speed rose to a higher value. The percentage difference between each model increased along with the rotational speed.

At a speed of 200 rpm, the BEMFs in the RMS value for the 18/20, 12/10, and 9/8 slot-poles were 35.9 V, 32 V, and 27.95 V, respectively. Furthermore, the 18/20 slot-pole had the highest value, whereas the 9/8 slot-pole had the lowest. The BEMF increased steadily with the rotational speed until 1000 rpm.

At the speed of 1000 rpm, the BEMFs for the 18/20, 12/10, and 9/8 slot-poles were 174.32 V, 141.11 V, and 120.94 V, respectively, demonstrating that the 18/20

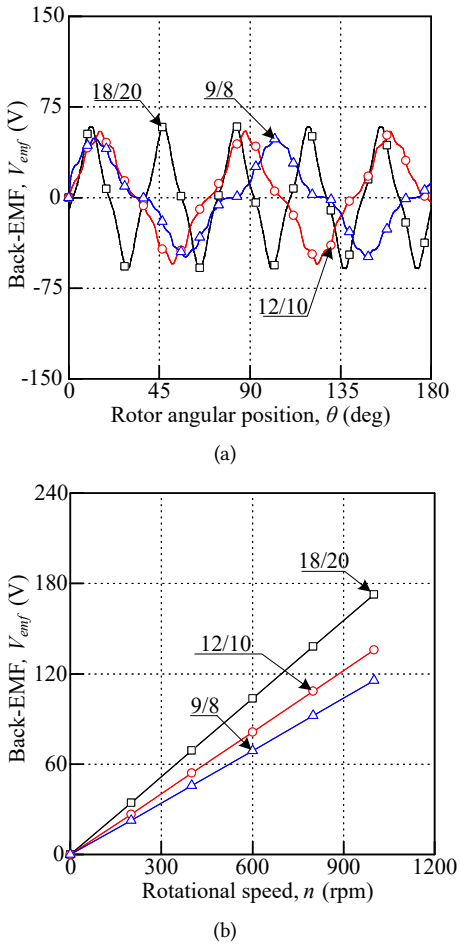

Fig. 13: Back-electromotive force; (a) waveform and (b) average value.

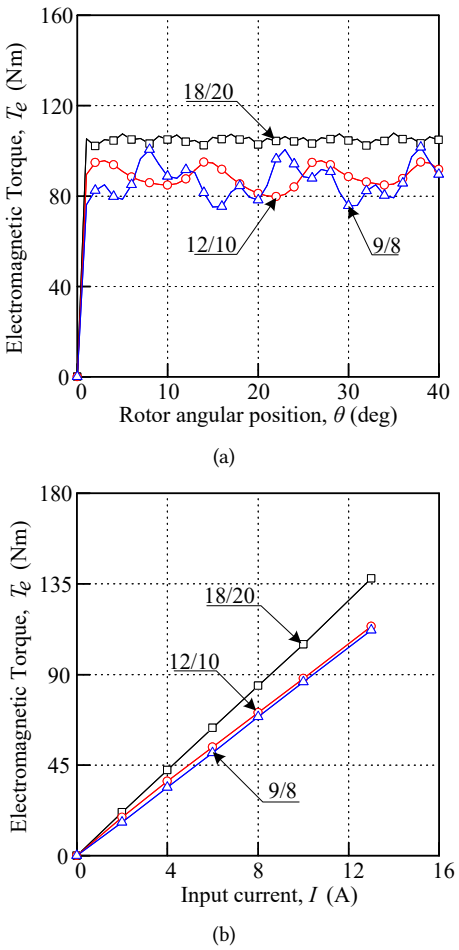

Fig. 14: Electromagnetic torque; (a) waveform and (b) RMS value.

slot-pole maintained the highest BEMF while the 9/8 remained the lowest.

To be exact, the 18/20 slot-pole model had the highest BEMF due to the higher number of slot and pole configurations compared to the other models, thus allowing it to produce the highest induced voltage.

As expected, the model with the higher slot-pole configuration had the ability to produce a higher BEMF compared to the other models and vice versa. This is because a greater number of poles produces a higher magnetic force.

4.3 Electromagnetic Torque

Fig. 14(a) shows the waveform of the electromagnetic torque (T_e) for different slot-pole models at 10 A. In the BLDC, the current control angle is a crucial component, playing a significant role in producing the electromagnetic torque. The phase current control angle must be aligned with the corresponding BEMF to obtain higher torque values.

Moreover, the 18/20 slot-pole had the lowest torque ripple and the 9/8 slot-pole the highest. This was possibly due to the slot and pole number factor, i.e., the higher the slot and pole number, the lower the torque ripple.

Since the number of slots and poles is bigger, it contributes to higher magnetic energy, keeping the torque going smoothly with the reduced torque ripple.

Furthermore, the 9/8 slot-pole was the highest due to its uneven air gap causing the rotor and stator to collide with each other and thus produce the highest torque ripple.

Fig. 14(b) shows the average electromagnetic torque value produced by all three models against the input currents (ranging from 2 A to 13 A). As can be observed, the electromagnetic torque produced by all models was nearly the same during the low input current and increased rapidly when the input current was higher.

At the moment when the input current was increased, the coil winding will be energized and produce electromagnetic energy. The higher the current being supplied, the higher its magnetic energy will be.

As a result, the electromagnetic produced will interact with the flux of the permanent magnets. The model with a larger number of slots and poles will have a smoother torque as the magnetic flux produced is closely distributed.

As can be observed, the electromagnetic torque obtained for all three models increased linearly in propor-

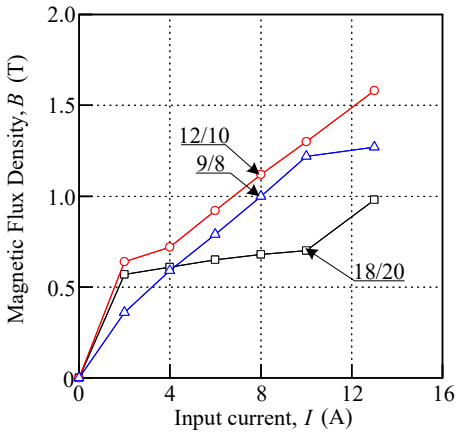

Fig. 15: *Magnetic flux density at the stator.*

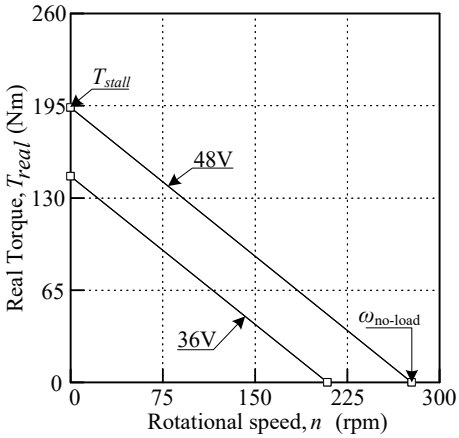

Fig. 16: *Torque-speed characterization of the 18/20 slot-pole model.*

Table 3: *Comparison of the model selection.*

Parameter	Model (slot/pole)		
	18/20	12/10	9/8
Cogging torque, T_C (Nm)	0.36	0.12	0.2
Back-EMF, V_{emf} (V)	35.9	32	27.95
Electromagnetic torque, T_e (Nm)	105	88	112
Magnetic flux density, B (T)	0.7	1.3	1.26

tion to the input current.

At 6 A, the torque of the 18/20 slot-pole started to exhibit a bigger difference compared to the others. Meanwhile, the 12/10 and 9/8 slot-poles only showed a slight difference, although the input current was up to 13 A and the values close to each other.

During an input current of 10 A, the average torque for the 18/20, 12/10, and 9/8 slot-poles was 105 Nm, 88 Nm, and 86.3 Nm, respectively, resulting in the 9/8 slot-pole producing the lowest torque.

As expected, the model with a larger number of slot-pole configurations had higher torque compared to the other models. This is because a larger number of slots and poles can contribute to higher magnetic energy for producing the torque.

In comparing the MMF for all three models, namely 36000 At, the average torque for the 9/8 slot-pole with an input current of 13 A is 112 Nm, thus producing the highest torque compared to the others.

4.4 Magnetic Flux Density

Fig. 15 shows the magnetic flux density (B) obtained for all three models against the input currents (ranging from 2 A up to a maximum of 13 A). As can be observed, the magnetic flux density for all models increases as the current input rises with different patterns. For the 18/20 slot-pole, starting from 2 A, its value increased slowly until the input current of 10 A, then rising suddenly at 13 A. Whereas the value of the 12/10 slot-pole showed a minimal increase from 2 A, rising rapidly until 13 A. Meanwhile, the value for the 9/8 slot-pole increased linearly with the input current and started to saturate at 10 A.

As tabulated in Fig. 15, the MMF concluded with 36000 At, while the magnetic flux density of the 18/20, 12/10, and 9/8 slot-poles was 0.7 T, 1.3 T, and 1.26 T, respectively. Overall, for 36000 At, the magnetic flux density of the 12/10 slot-pole was the highest compared to the others. The 18/20 slot-pole was expected to be the highest but turned out to be the lowest because it achieved the optimum magnetic energy level.

4.5 Performance Comparison

Table 3 shows the comparison between the cogging torque and BEMF at a constant speed of 200 rpm. The electromagnetic torque and magnetic flux density for MMF of 36000 At are also presented. The proposed 18/20 slot-pole model configuration was found to be the best model for selection. Although it had the lowest magnetic flux density, it was able to produce the highest BEMF. On the other hand, even though the torque of the 9/8 slot-pole model was higher than that of the 18/20 during an MMF of 36000 At, it was unacceptable due to the heat factor with the high input current being 13 A. Therefore, the torque value of the 18/20 slot-pole model was chosen with 105 Nm at an input current of 10 A only. With a percentage difference of 6.25% compared to 112 Nm at 13 A for the 9/8 slot-pole model, the 18/20 slot-pole model was selected as the most suitable model for agro-EV motor application.

4.6 Torque-Speed Characterization

Fig. 16 shows the real torque vs. speed characterization of the 18/20 slot-pole model for agro-EV. When applying 48 V to the motor, the stall torque, T_{stall} produced by the BLDC motor, is 193.67 Nm during a standstill. This is the point at which the torque and current are maximized. Meanwhile, the speed with no load, $\omega_{no-load}$ is 277.46 rpm. This is the maximum speed that the motor can achieve at a given voltage in an ideal case, where no torque is generated. When lower voltages are applied, the T_{stall} and $\omega_{no-load}$ will achieve lower

values. In reality, the maximum operation of torque depends on the ratio of the input power to the total loss of the motor, which will eventually cause rotor misstep from the following coil current pattern. This makes the rotor stop rotating.

5. CONCLUSION

In conclusion, the proposed models, namely the 18/20, 12/10, and 9/8 slot-poles, were designed with a fixed air gap, and rotor and stator sizing. The transient magnetic application analysis was carried out using the FEM. The selection of the best model focused on the highest BEMF and electromagnetic torque value. The 18/20 slot-pole model was found to be the best. Based on its torque-speed characteristic, the 18/20 slot-pole model was able to produce high torque during low speed for agro-EV application. This paper shows that the performance of the BLDC motor was affected by the number of slot and pole configurations. A larger slot-pole number will produce higher BEMF and electromagnetic torque. Based on the findings of this research, some methods and design recommendations can be used for future research to improve the performance of the PM BLDC motor. The recommendations are as follows:

1. The use of an appropriate design and stator tooth width can contribute to reducing the cogging torque.
2. The slot opening width for the stator should be larger to fill the space with a greater number of turns.
3. The inner diameter of the stator and outer diameter of the rotor should be designed more accurately to give a precise and uniform air gap to prevent a collision.
4. Bigger slot-pole numbers can increase the magnetic flux density since the magnets are closely embedded, contributing to a higher BEMF and torque value.

Furthermore, the study of BLDC vibration could also have a positive impact on the design and analysis of the BLDC motor in future research. Hopefully, these recommendations can improve the torque produced and the PM BLDC motor performance.

ACKNOWLEDGMENTS

The authors would like to thank the Ministry of Higher Education Malaysia, Universiti Teknikal Malaysia Melaka (UTeM), for providing the research grants MTUN/2019/FKE-CERIA/MC0003. The authors would also like to acknowledge the support from Altair Engineering Sdn. Bhd. for providing the Altair Flux 2D software for this research.

Author Contributions: Raja Nor Firdaus Kashfi Raja Othman and Muhammad Izanie Kahar conceived and designed the simulations; Aziah Khamis, Nurfaezah Abdullah, Fairul Azhar Abdul Shukor, and Lim Seng Tat contributed to the analysis and Altair Flux 2D software.

REFERENCES

[1] J. Larminie and J. Lowry, *Electric Vehicle Technology Explained*. Hoboken, NJ, USA: John Wiley & Sons, 2003.

[2] M. Yildirim, M. Polat, and H. Kurum, "A survey on comparison of electric motor types and drives used for electric vehicles," in *2014 16th International Power Electronics and Motion Control Conference and Exposition*, 2014, pp. 218–223.

[3] C. C. Chan, "Present status and future trends of electric vehicles," in *1993 2nd International Conference on Advances in Power System Control, Operation and Management, APSCOM-93.*, vol. 1, 1993, pp. 456–469.

[4] F. L. Luo and H. G. Yeo, "Advanced PM brushless DC motor control and system for electric vehicles," in *Thirty-Fifth IAS Annual Meeting and World Conference on Industrial Applications of Electrical Energy*, vol. 2, 2000, pp. 1336–1343.

[5] A. Tashakori, M. Ektesabi, and N. Hosseinzadeh, "Modeling of BLDC motor with ideal back-EMF for automotive applications," in *Proceedings of the World Congress on Engineering 2011 (WCE 2011)*, vol. II, London, UK, 2011, pp. 1504–1508.

[6] X. D. Xue, K. W. E. Cheng, and N. C. Cheung, "Selection of electric motor drives for electric vehicles," in *2008 Australasian Universities Power Engineering Conference*, 2008.

[7] N. Hashemnia and B. Asaei, "Comparative study of using different electric motors in the electric vehicles," in *2008 18th International Conference on Electrical Machines*, 2008.

[8] T. Yabe, K. Akatsu, N. Okui, T. Niikuni, and T. Kawai, "Efficiency improvement of regenerative energy for an EV," *World Electric Vehicle Journal*, vol. 5, no. 2, pp. 494–500, 2012.

[9] L. Andaloro, G. Napoli, F. Sergi, S. Micari, G. Agnello, and V. Antonucci, "Development of a new concept electric vehicle for last mile transportations," *World Electric Vehicle Journal*, vol. 7, no. 3, pp. 342–348, 2015.

[10] P. Wach, "Brushless DC motor drives (BLDC)," in *Dynamics and Control of Electrical Drives*. Berlin, Germany: Springer, 2011, pp. 281–380.

[11] J. West, "DC, induction, reluctance and PM motors for electric vehicles," *Power Engineering Journal*, vol. 8, no. 2, pp. 77–88, Apr. 1994.

[12] G. Nanda and N. Kar, "A survey and comparison of characteristics of motor drives used in electric vehicles," in *2006 Canadian Conference on Electrical and Computer Engineering*, 2006, pp. 811–814.

[13] J. Xintong, X. Jingwei, L. Yong, and L. Yongping, "Theoretical and simulation analysis of influences of stator tooth width on cogging torque of BLDC motors," *IEEE Transactions on Magnetics*, vol. 45, no. 10, pp. 4601–4604, Oct. 2009.

[14] K. Krykowski and J. Hetmańczyk, "Constant current models of brushless DC motor," *Electrical, Control*

and Communication Engineering, vol. 3, no. 1, pp. 19–24, 2013.

[15] Y. Jeon, H. Mok, G. Choe, D. Kim, and J. Ryu, "A new simulation model of BLDC motor with real back EMF waveform," in *Proceedings of the 7th Workshop on Computers in Power Electronics (COMPEL 2000)*, 2000, pp. 217–220.

[16] P. Kumar and P. Bauer, "Improved analytical model of a permanent-magnet brushless DC motor," *IEEE Transactions on Magnetics*, vol. 44, no. 10, pp. 2299–2309, Oct. 2008.

[17] B. K. Ahirwal, K. K. Pandey, and J. S. Bhadoriya, "A novel approach of rotor position detection of a sensorless BLDC motor with improved back EMF," *International Journal of Advanced Research in Electrical, Electronics and Instrumentation Engineering*, vol. 3, no. 11, pp. 12 901–12 908, Nov. 2014.

[18] A. Thakur, "Improvement of back EMF & minimization of torque ripple of BLDC motor," *IJO-Science*, vol. 5, no. 8, pp. 1–7, Aug. 2019.

[19] K.-J. Han, H.-S. Cho, D.-H. Cho, and H.-K. Jung, "Optimal core shape design for cogging torque reduction of brushless DC motor using genetic algorithm," *IEEE Transactions on Magnetics*, vol. 36, no. 4, pp. 1927–1931, Jul. 2000.

[20] G.-H. Kang, J. Hur, H.-G. Sung, and J.-P. Hong, "Optimal design of spoke type BLDC motor considering irreversible demagnetization of permanent magnet," in *Sixth International Conference on Electrical Machines and Systems (ICEMS 2003)*, vol. 1, 2003, pp. 234–237.

[21] H.-S. Kim, Y.-M. You, and B.-I. Kwon, "Rotor shape optimization of interior permanent magnet BLDC motor according to magnetization direction," *IEEE Transactions on Magnetics*, vol. 49, no. 5, pp. 2193–2196, May 2013.

[22] A. S. Cabuk, S. Saglam, and O. Ustun, "Impact of various slot-pole combinations on an in-wheel BLDC motor performance," *Electrica*, vol. 17, no. 2, pp. 3369–3375, Jul. 2017.

[23] I. Garniwa, B. Dipantara, M. V. Nugroho, B. Sudiarto, and N. Noorfatima, "Analysis of the effect of the motor temperature to brushless direct current motor performance on KARLING electric vehicle," *Journal of Physics: Conference Series*, vol. 1376, 2019, Art. no. 012024.

[24] J. Krotsch and B. Piepenbreier, "Radial forces in external rotor permanent magnet synchronous motors with non-overlapping windings," *IEEE Transactions on Industrial Electronics*, vol. 59, no. 5, pp. 2267–2276, May 2012.

[25] J. R. Hendershot and T. J. E. Miller, *Design of Brushless Permanent-magnet Machines*. Hillsboro, OH, USA: Magna Physics Pub., 1994.

Muhammad Izanie Kahar received the B.Eng. in Electrical Engineering in 2020 from Universiti Teknikal Malaysia Melaka. Currently, he is pursuing his study in M.Sc. at the same university. His interest of research is analysis in electrical machine design.

Raja Nor Firdaus Kashfi Raja Othman received his B.Eng., M.Sc., and Ph.D. in Electrical Power Engineering from Universiti Putra Malaysia in 2006, 2009, and 2013, respectively. He is currently an associate professor in Department of Electrical Engineering, Faculty of Electrical Engineering, Universiti Teknikal Malaysia Melaka. His research interest includes applied magnetics, electrical machines, magnetic sensor and drives.

Aziah Khamis received the B.Eng. degree from Universiti Putra Malaysia in 2006. Then, M.Sc. degree from Newcastle University, U.K. in 2009. Later, Ph.D. degree from Universiti Kebangsaan Malaysia in 2014. She is a senior lecturer at Universiti Teknikal Malaysia Melaka. Her main research interests include intelligent system application of power system study, distributed generation, and microgrid.

Nurfaezah Abdullah received her B.Eng. in Power Electronics and Drives in 2012 and M.Sc. Electrical Engineering at Universiti Teknikal Malaysia Melaka. Currently, she is pursuing her Ph.D. studies at Universiti Teknikal Malaysia Melaka. Her research interest includes the field in machine design, photovoltaic system, and power electronics.

Fairul Azhar Abdul Shukor received his B.Eng in Electrical and Electronic Engineering from Universiti Putra Malaysia in 2002. Then, D.Eng. in Electrical Machine Design from Shinshu University, Nagano, Japan in 2015. He currently senior lecturer at Department of Power Electronis and Drives, Faculty of Electrical Engineering, Universiti Teknikal Malaysia Melaka. His research interest includes electrical machines, magnetic sensor, machine design, and electric vehicle.

Lim Seng Tat started the career as CAE engineer for automotive industry. He is sales director of Altair Engineering in charge of Malaysia and Philippines. He had conducted more than 100 of workshops, trainings and technology events across ASEAN region with covered the topics across different industries including automotive, aerospace, manufacturing, electronics, appliance, defense, etc. Now, he currently focuses in business development on both Malaysia and Philippines.